Direct spectroscopic evidence of photoisomerization in *para*-methoxy methylcinnamate revealed by low-temperature matrix-isolation FTIR spectroscopy

Yasunori Miyazaki,[†] Yoshiya Inokuchi,[†] Nobuyuki Akai[‡], and Takayuki Ebata,[†*]*

[†]Department of Chemistry, Graduate School of Science, Hiroshima University, Higashi-Hiroshima 739-8526, Japan

[‡]Graduate School of Bio-Applications and Systems Engineering (BASE), Tokyo University of Agriculture and Technology, Naka-cho, Koganei, Tokyo 184-8588, Japan

Abstract

The photoisomerization of *para*-methoxy methylcinnamate (*p*-MMC) has been studied by low-temperature matrix-isolation FTIR spectroscopy. In particular, the difference spectrum of mid-IR frequency region (1100–1800 cm^{-1}) allows us to distinguish the structural change before and after ultraviolet (UV) light irradiation at ≥300 nm and to convince that the *cis*-isomer is produced from the *trans*-isomer by comparing with the calculated IR spectra. Additionally, a reversible isomerization of *p*-MMC is demonstrated upon a sequential irradiation with different wavelengths of UV light. These findings provide a new insight of the electronic excited state dynamics of *p*-MMC.

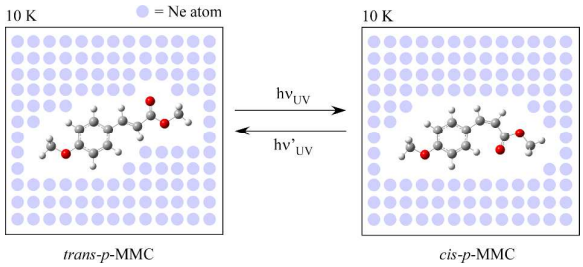

Table of Content

Photoisomerization of a protein chromophore controls molecular/protein dynamics that evolves selective biological activity in response to a certain wavelength of light. One of the most well-known chromophores is retinal found in rhodopsin because the primary event in vision is triggered by rotating the conjugated double bond at the 11-*cis* position to form all-*trans* configuration.[1-4]The mapping of the potential energy surface at around the S_1/S_0 conical intersection has been searched experimentally[5-6] and theoretically[7-8] for elucidating its unique reactivity. The fluorescent protein has also been studied since its discovery of the green fluorescent protein from *Aequorea victoria* and its fluorescent protein analogs from *Anthozoa* and *Pectiniidae*.[9-11] They hold a chromophore of 4-(*p*-hydroxybenzylidene)-5-imidazolinone (*p*-HBI) that isomerizes reversibly and switches fluorescence on and off when the *cis* and *trans* are excited, respectively.[12] The advanced protein technology improves the range of color region as well as brightness of fluorescence, both of which are succeeded in vivo imaging of cells and tissues in biomedical field.[13-16] Another example is *p*-coumaric acid embedded in the Photoactive Yellow Protein (PYP).[17-20] It features a thio-ester linkage to the amino acid residue that gives rise to a shift of the absorbing wavelength toward the blue light.[21] It is understood that the light-induced isomerization together with the protonation in the anionic phenolic oxygen initiates the photocycle and results in negative phototaxis behavior in *halophilia*.

The selective bond isomerization has motivated several studies on the dynamics of not only a protein but also an isolated chromophore. We have been studying the electronic state dynamics of methylcinnamate derivatives in gas phase, which are recognized as a PYP model chromophore.[22,23] So far, two initial decay mechanisms are proposed by a combination of lifetime measurement[22-25] and theoretical calculation[26-27]

but no decisive conclusion has been reached yet. In this letter, we report an attempt to ensure the occurrence of the *trans*↔*cis* photoisomerization of *para*-methoxy methylcinnamate (*p*-MMC) by using low-temperature matrix-isolation FTIR spectroscopy.

Figure 1(a) shows the recorded IR spectrum of *p*-MMC deposited on the low-temperature Ne matrix in the frequency region of 1100–1800 cm^{-1} before UV light is irradiated. Almost all sharp bands are assigned by the comparison with the calculated IR spectra of the *s-cis/anti*, *s-cis/syn*, *s-trans/anti* and *s-trans/syn* conformers of *trans-p*-MMC as shown in Figures 1(b), (c), (d) and (e), respectively. The IR frequency and vibrational mode assignment are summarized in Table 1. In particular, the strong band **A** at 1172 cm^{-1} is characteristics of the *s-cis* conformer (Figures 1(b) and (c)), which is assigned to the C-O stretch of the ester group. The *s-trans* conformer, on the other hand, has the ester C-O stretch at the weak band **B** 1257 cm^{-1} as predicted in Figures 1(d) and (e). Therefore, we deduced that the *s-cis* conformer is predominated over the *s-trans* conformer from the relative band intensities between the observed and calculated spectra. The S_0 state stability among the conformers listed in Table 2 supports our deduction. The *trans/s-trans*/(*anti* or *syn*) conformers are ~300 cm^{-1} higher in energy than the *trans/s-cis*/(*anti* or *syn*) conformers. The previous studies on cold rare gas matrix revealed that interconversion among the conformers doe not occur during the deposition[28-30], so that we can assume their relative population is preserved to that before the deposition. The Boltzmann distribution at vaporization temperature 302 K (29 °C) yields 0.22 population ratio of the *s-trans* conformer to the *s-cis* conformer, which is in good agreement with the relative band intensity of the ester C-O stretch

between 1257 cm^{-1} (*s-trans*) and 1172 cm^{-1} (*s-cis*) of the observed spectrum. The energy difference between *anti* to *syn* conformer is very small (57 cm^{-1}), and band positions are almost identical except the band E of *anti*-conformer at 1585 cm^{-1}. The population ratio of *anti* to *syn* was estimated by focusing on the reversed order of the band intensities at 1293 cm^{-1}, 1306 cm^{-1}, 1318 cm^{-1} and 1331 cm^{-1} as predicted in the calculation (Figures 1 (b) and (c)). These bands exhibit equal intensity in the observation (Figure 1(a)). It implies that *anti* and *syn* conformers coexist almost equally under the present condition.

Figure 2(a) shows the difference IR spectrum of *p*-MMC obtained by subtracting the IR spectrum before UV light irradiation from the one after 2-minute UV light irradiation with $\lambda_{UV} \geqq 300$ nm. The 0,0 band of the *s-cis/syn* conformer of *trans-p*-MMC is located at 32328 cm^{-1} in gas phase.[23] Since the perturbation of the electronic state by Ne is thought to be small, the electronic transition energy is almost unchanged from the gas phase value. Thus, *p*-MMC is predominantly excited to the $S_1(\pi\pi^*)$ state. In the difference spectrum, the downward and upward bands indicate the reactant and the photoproduct, respectively. It is obvious that the vibrational frequencies of the photoproduct are all lower than the reactant ones as highlighted in grey in Figure 2, i.e. band A at 1170 cm^{-1} (C-O stretch of the ester group), band D at 1517 cm^{-1} (C-H bend of the ring), band H at 1645 cm^{-1} (C=C stretch of the propenyl group), and band I(I') at 1740 cm^{-1} (C=O stretch of the carbonyl group), where the prime means the product vibration. To identify the photo-product, we calculated the *cis-p*-MMC as the most probable candidate. Figures 2(b)-(e) show the difference IR spectra between the various *cis*-isomer products and the *trans/s-cis/anti* conformer with 1:1 correspondence, where the calculated structures and IR spectra of *cis*-isomers are shown in Figure 3 (a)-(d)). Of

all, the *cis/s-cis/(anti and syn)* conformers in Figures 2 (b) and (c) reproduce the experimental spectrum having the upward band A'(1167 cm^{-1}), band D'(1503 cm^{-1}), band H'(1630 cm^{-1}), and band I'(1740) cm^{-1}) , which are shifted by 5~10 cm^{-1} from the *trans/s-cis/anti* conformer. The missing difference at 1172 cm^{-1} in Figure 2(b) is due to a cancelation of the identical IR frequency between the *trans/s-cis/anti* and *cis/s-cis/anti* conformers (Figure 3(a)). In contrast, the difference of the calculated IR spectra in Figures 2(d) and (e) showing the single downward band at 1172 cm^{-1} is rather poor. The difference IR spectra using the *trans/s-cis/syn* conformer resembles Figures 2 (b)-(e), providing a concrete evidence that *cis*-isomer is produced upon UV light irradiation. ***It is noteworthy that we observed the C=C stretch band of the propenyl group of the cis-isomer at 1630 cm^{-1} (band H'), which is slightly shifted from the trans-isomer at 1644 cm^{-1}(band H).***

In the *s-cis* conformers shown in Figure 3, the *ortho* C-H of the aromatic ring is attracted to the lone pair electrons of the carbonyl oxygen retaining the molecular plane. In the *s-trans* conformers, on the other hand, it is interacted with the lone pair electrons of the C-O oxygen that causes a distortion at the dihedral angle of C=C bond. Such geometric factor largely influences the S_0 state stability as seen in Table 2. In addition, the energy barrier from *s-trans* to *s-cis* in the *cis*-isomer in the S_0 state is estimated to be ~700 cm^{-1}, which suggests that the conformational interconversion takes place even if the *cis/s-trans/(anti or syn)* conformers are initially produced. Taken together, we conclude that the *cis/s-cis/(anti and syn)* products are produced from the *trans/s-cis/(anti and syn)* reactant by photoisomerization. Finally, the possibility of a light-induced single-bond rotation in the *trans*-isomer is discussed. As mentioned above, the *trans/s-trans* conformer exhibits the strong ester C-O stretch band at 1265 cm^{-1}.

There is no such band in the observed spectrum so that we crossed out the *s-trans/anti* conformer as a photoproduct.

The backward isomerization of the *cis*-photoproduct was promoted by irradiating additional UV light with $\lambda_{UV} \geqq 275$ nm for 30 seconds after the UV ($\lambda_{UV} \geqq 300$ nm) light irradiation. By doing so, the molecules will be excited not only to the first $^1\pi\pi^*$ state but also to $^1n\pi^*$ and second $^1\pi\pi^*$ states.[23,26] Figure 4(c) shows the difference spectrum between the IR spectrum of the sample with $\lambda_{UV} \geq 300$ nm irradiation (Figure 4(b)) and the one with $\lambda_{UV} \geq 300$ nm and $\lambda_{UV} \geq 270$ nm irradiation. The bands of *cis*-photoproduct are depleted and new upward bands appear at slightly higher frequency side. The upward bands can be assigned to the *trans/s-cis/(anti or syn)* conformer, that is the initial reactant. Figure 4(d) shows the difference IR spectrum between the sequential UV ($\geqq 300$ nm + $\geqq 275$ nm) light irradiation and without the UV light irradiation. The IR spectrum in Figure 4(d) is almost identical to one in Figure 4(a). Thus, the final product is again the *trans/s-cis/(anti or syn)* conformer or the initial reactant. It indicates no undesirable conformation change e.g. *s-cis* → *s-trans* occurs during the reversible photoisomerization process. These results suggest that all these reactions occur very rapidly and are controlled dynamically on the potential energy surface. If the statistically slow reaction takes place, the *trans/s-trans* conformer will be produced in the backward photoisomerization reaction because there is no geometrical constraint to interconvert *trans/s-trans* and *trans/s-cis* conformers. The other intriguing issue is that the forward reaction (*trans* → *cis*) occurs in the S_0 state but the backward reaction (*cis* → *trans*) preferentially occurs by 275 nm UV light irradiation. The second $^1\pi\pi^*$ state or even higher electronic excited state may play an important role in the backward

reaction.

In conclusion, we investigated the photoisomerization of *p*-MMC by low-temperature matrix-isolation FTIR spectroscopy. It was found that *trans*→*cis* photoisomerization occurs in the S_1 state as the matrix-cooled sample was irradiated with the wavelength of light longer than 300 nm. The formation of the *cis*-photoproduct was identified by the characteristic lower frequency shifts of the IR bands of the C-O stretch of the ester group, C-H bend of the aromatic ring, C=C stretch of the propenyl group, and C=O stretch of the carbonyl group. Furthermore, *cis*→*trans* backward photoisomerization was observed by the irradiation of UV light longer than 275 nm to the isomerized product. Thus, it is confirmed that the *cis*↔*trans* photoisomerization is a reversible process. The photoproducts show a preference in the population ratio of conformers, indicating the reactions are dynamically controlled on the potential energy surface rather than statistically controlled. Extension of this study is in progress, and we hopefully provide the general trend of the *cis*↔*trans* photoisomerization reaction in other cinnamate derivatives such as OMpCA and methylcinnamate and so on.

Methodology

The white powdery *p*-MMC was vaporized at 29 °C and deposited with neon gas on a CsI plate cooled by a closed-cycle helium refrigerator (Iwatani, Cryo Mini) at 6 K. Two hours were spent to prepare the matrix sample. Infrared (IR) spectra of the matrix-isolated sample were recorded in the range of 700-4000 cm^{-1} by an FTIR spectrophotometer (JEOL, SPX200ST) with an accumulation number of 100. The spectral resolution is 0.5 cm^{-1}. A xenon lamp (Asahi Spectra, MAX-301uv) was used as an ultraviolet (UV) light source and was narrowed by using two types of a

short-wavelength cutoff filter. One is LU0300 (Asahi Spectra Co. Ltd.) for the λ_{UV} ≧300 nm irradiation experiment where the transmission efficiency at 300 nm, 296 nm and 290 nm is 50 %, 10 % and 0.8 %, respectively. The other is a combination of LU0275 (Asahi Spectra Co. Ltd.) and LU0250 (Asahi Spectra Co. Ltd.) for λ_{UV} ≧275 nm irradiation experiment where the transmission efficiency at 275 nm, 272 nm and 268 nm is 50 %, 10 %, and 0.8 %, respectively. These cutoff filters were combined to generate λ_{UV} ≧275 nm of light, making it for the experiment.

Quantum chemical calculations were performed in the Gaussian 09 program package. Four conformers exist in each isoform of *p*-MMC. The notations *syn* and *anti* represents the orientation of the -OMe group with respect to the substituent in the opposite side of the ring, and the notations *s-cis* and *s-trans* differ the internal rotation of the single bond between C=C and C=O. All conformations of the *trans*-isomer were optimized in the C_s symmetry while *s-cis/(anti or syn)* and *s-trans/(anti or syn)* of the *cis*-isomer were optimized in the C_s symmetry and C_1 symmetry, respectively. Several density functionals such as B3LYP, cam-B3LYP and M06-2X with the 6-311++G(d,p) basis set and PBE0 with the cc-pVDZ basis set were tested to validate their conformational stabilities and IR spectra. The comparative S_0 state energy is obtained among the functionals, giving the same order of the stability (data not shown). The B3LYP-calculated IR spectra (a scaling factor of 0.9941) best reproduced the experimental ones. In what follows, calculation result is the B3LYP/6-311++G(d, p) level of theory. The *cis*-isomer is ~1700 cm^{-1} higher in energy than the *trans*-isomer (Table 2), and the barrier height to interconvert between them is >10000 cm^{-1}. Such a high energy barrier allowed us to postulate a negligibly small population of the

cis-isomer in the sample matrix without UV light irradiation.

Acknowledgements

T. E. acknowledges Japan Society for the Promotion (JSPS) for the support through a Grand-in-Aid project (No. 25410017).

References

1. George R. C. C. Sr. THE INTERPLAY OF LIGHT AND HEAT IN BLEACHING RHODOPSIN. *J. Gen. Physiol.* **1952**, 35, 495-517.

2. Kandori H.; Sasabe H.; Nakanishi K.; Yoshizawa T.; Mizukami T.; Shichida Y. Read-Time Detection of 60-fs Isomerization in a Rhodopsin Analog Containing Eight-Membered-Ring Retinal. *J. Am. Chem. Soc.* **1996**, 118, 1002-1005.

3. Kandori H.; Matuoka S.; Shichida Y.; Yoshizawa T.; Ito M.; Tsukida K.; Balogh-Nair V.; Nakanishi K. Mechanism of Isomerization of Rhodopsin Studied by Use of 11-Cis-Locked Rhodopsin Analogues Excited with a Picosecond Laser Pulse. *Biochemistry.* **1989**, 28, 6460-6467.

4. Imasheva E. S.; Balashov. S. P.; Wang J. M.; Dioumaev A. K.; Lanyi J. K. Selectivity of Retinal Photoisomerization in Proteorhodopsin Is Controlled by Aspartic Acid 227. *Biochemistry*, **2004**, 43, 1648-1655.

5. Polli D.; Atoè P.; Weingart W.; Spillane K. M.; Manzoni C.; Brida D.; Tomasselo G.; Orlandi G.; Kukura P.; Mathies R. A.; Garavelli M.; Cerullo G. Conical intersection dynamics of the primary photoisomerization event in vision *Nature*. **467**, 440-443.

6. Zgablic G.; Novello A. M.; Parmiginani F. Population Branching in the Conical Intersection of the Retinal Chromophore revealed by Multipulse Ultrafast Optical

Spectroscopy. *J. Am. Chem. Soc.* **2012**, 134, 955-961.

7. Send R.; Sundholm D. Stairway to the Conical Intersection: A Computational Study of the Retinal Isomerization. *J. Phys. Chem.* A **2007**, 111, 8766-8773.

8. Aquino A. J. A.; Barbatti M.; Lischka H. Excited-State Properties and Environmental Effects for Protonated Schiff bases: A Theoretical Study. *ChemPhysChem.* **2006**, 7, 2089-2096.

9. Shimomura O.; Johnson F. H.; Saiga Y. Extraction, purification and properties of aequorin, a bioluminescent protein from the luminous hydromedusan, Aequorea. *J. Cell. Comp. Physiol.* **1962**, 59, 223-239.

10. Matz M. V.; Fradkov A. F.; Labas Y. A.; Savitsky A. P.; Zaraisky A. G.; Markelov M. L.; Lukyanov S. A. Fluorescent proteins from nonbioluminescent Anthozoa species. *Nature Biotechnology* **1999**, 17, 969-973.

11. Ando R.; Mizuno H.; Miyawaki A.; Regulated fast nucleocytoplasmic shuttling observed by reversible protein highlighting. *Science* **2004**, 306, 1370-1373.

12. Anderesen M.; Wahl M. C.; Stiel A. C.; Gräter F.; Schäfer L. V.; Trowitzsch S.; Weber G.; Eggeling C.; Grubmüller H.; Hell S. W.; Jakobs S. Structure and mechanism of the reversible photoswitch of a fluorescent protein. *PNAS* **102**, 13070-13074.

13. Betzig E.; Patterson G. H.; Sougrat R.; Lindwasser O. W.; Olenych S.; Bonifacino J. S.; Davidson M. W.; Lippincott-Schwarts J.; Hess H. F. Imaging intracellular fluorescent proteins at nanometer resolution. *Science* **2006**, 313, 1642-1645.

14. Hess S. T.; Girirajan T. P.; Mason M. D. Ultra-high resolution imaging by fluorescence photoactivation localization microscopy. *Biophys J.* **2006**, 91, 4258-4272.

15. Chalfie M.; Tu Y.; Euskirchen G.; Green fluorescent protein as a marker for gene expression. *Science*, **1994**, 263, 802-805.

16. Chudakov D. M.; Belousov V. V.; Zaraisky A. G.; Novoselov V. V.; Staroverov D. B.; Zorov D. B.; Lukyanov S.; Lukyanov K. A. Kindling fluorescent proteins for precise in vivo photolabeling. *Nat. biotechnol.* **2003**, 21, 191-194.

17. Hoff W. D.; Düx P.; Hård K.; Devreese B.; Nugteren-Roodzant I. M.; Crielaard W.; Boelens R.; Kaptein R.; Beeumen J. V.; Hellingwerf K. J. Thiol Ester-Linked *p*-Coumaric Acid as a New Photoactive Prosthetic Group in a Protein with Rhodopsin-Like Photochemistry. *Biochemistry* **1994**, 33, 13959-13962.

18. Carroll E. C.; Hospes M.; Valladares C.; Hellingwerf K. J. Larsen D. S. Is the photoactive yellow protein a UV-B/blue light photoreceptor? *Photochem. Photobiol. Sci.* **2011**, 10, 464-468.

19. Jung Y. O.; Lee J. H.; Kim J.; Schmidt M.; Moffat K.; Šrajer V.; Ihee H. Volume-conserving *trans-cis* isomerization pathways in photoactive yellow protein visualized by picosecond X-ray crystallography. *Nature Chemistry* **2013**, 5, 212-220.

20. Düx P.; Rubinstenn G.; Vuister G. W.; Boelens R.; Mulder F. A. A.; Hård K.; Hoff W. D.; Kroon A. R.; Crielaard W.; Hellingwerf K. J.; Kaptein R. Solution Structure and Backbone Dynamics of the Photoactive Yellow Protein. *Biochemistry* **1998**, 37, 12689-12699.

21. Vengris M.; Larsen D. S.; Horst M. A. V.; Larsen O. F. A.; Hellingwerf K. J.; Grondelle R. V. Ultrafast Dynamics of Isolated Model Photoactive Yellow Protein Chromophores: "Chemical Perturbation Theory" in the Laboratory. *J. Phys. Chem.* B **2005**, 109, 4197-4208.

22. Shimada D.; Kusaka R.; Inokuchi Y.; Ehara M.; Ebata T. Nonradiative decay dynamics of methyl-4-hydroxycinnamate and its hydrated complex revealed by picosecond pump-probe spectroscopy. *Phys. Chem. Chem. Phys.* **2012**, 14, 8999-9005.

23. Miyazaki Y.; Kanji Yamamoto, K.; Aoki, J.; Ikeda, T.; Inokuchi, Y.; Ehara, M.; Ebata, T. Experimental and theoretical study on the excited-state dynamics of *ortho*-, *meta*-, and *para*-methoxy methylcinnamate, *J. Chem. Phys.* **2014**, 141, 244313.

24. Tan E. M. M.; Amirjalayer S.; Bakker B. H.; Buma W. J. Excited state dynamics of Photoactive Yellow Protein chromophores elucidated by high-resolution spectroscopy and ab initio calculations. *Faraday Discuss.* **2013**, 163, 321-340.

25. Tan E. M. M.; Hilbers M. Buma W. J. Excited-State Dynamics of Isolated and Microsolvated Cinnamate-Based UV-B Sunscreens. *J. Phys. Chem. Lett.* **2014**, 5, 2464-2468.

26. Promkatkaew M.; Suramitr S.; Karpkird T. M.; Namuangruk S.; Ehara M. Absorption and emission spectra of ultraviolet B blocking methoxy substituted cinnamates investigated using the symmetry-adapted cluster configuration interaction method. *J. Chem. Phys.* **2009**, 131, 224306.

27. Gromov E. V.; Burghardt I.; Köppel H.; Cederbaum L. S. Impact of Sulfer vs Oxygen on the Low-Lying Excited States of *trans-p*-Coumaric Acid and *trans-p*-Coumaric Thio Acid. *J. Phys. Chem.* A **2005**, 109, 4623-4631.

28. Akai N.; Ohno K.; Aida M. Photochemistry of 2-(methylamino)pyridine in a low temperature argon matrix: Amino-imino tautomerism and rotational isomerism. *J. Photochem. Photobiol.*, A **2007**, 187, 113-118.

29. Akai N.; Kudoh S.; Nakata M. Methyl-Group Move in Low-Temperature Rare-Gas Matrixes and Conformational Analysis of 1,4-Dimethoxybenzene. *J. Phys. Chem.* A **2003**, 107, 2635-2641.

30. Nishino S.; Nakata M. Intramolecular Hydrogen Atom Tunneling in 2-Chlorobenzoic Acid Studied by Low-Temperature Matrix-Isolated Infrared

Spectroscopy. *J. Phys. Chem.* A **2007**, 111, 7041-7047.

Figure captions

Figure 1. (a) IR spectrum of *p*-MMC deposited on the low-temperature Ne matrix without UV irradiation. The letters A - I indicate the major vibrational bands in the mid-IR region. (b)-(e) calculated IR spectra of *trans-p*-MMC conformers and molecular structures (inlet). A scaling factor of 0.9941 was applied to correlate the 1172 cm^{-1} band (band A) of the observed spectrum.

Figure 2. (a) Difference IR spectrum of *p*-MMC between the UV (> 300 nm) iradaited one and that before the UV irradiation, on the low-temperature Ne matrix. (b)-(e) calculated difference IR spectra of *p*-MMC obtained by subtracting the *trans/s-cis/anti* conformer from the *cis/s-cis/(anti or syn)* conformer. Each spectrum was scaled with a factor of 0.9941. The grey colored regions highlight the remarkable structural change.

Figure 3. (a)-(d) Calculated IR spectra of *cis-p*-MMC conformers (left) and molecular structures with the top and side views (right)

Figure 4. (a) IR spectrum of *p*-MMC before the UV irradiation. (b) Difference IR spectrum of *p*-MMC between the UV (> 300 nm) iradaited one and that before the UV irradiation. (c) ifference IR spectrum of *p*-MMC between the sequential UV (> 300 nm + > 275 nm) iradaited one and that of the UV (> 300 nm) irradaited. (d) Difference IR spectrum between (c) and (a).

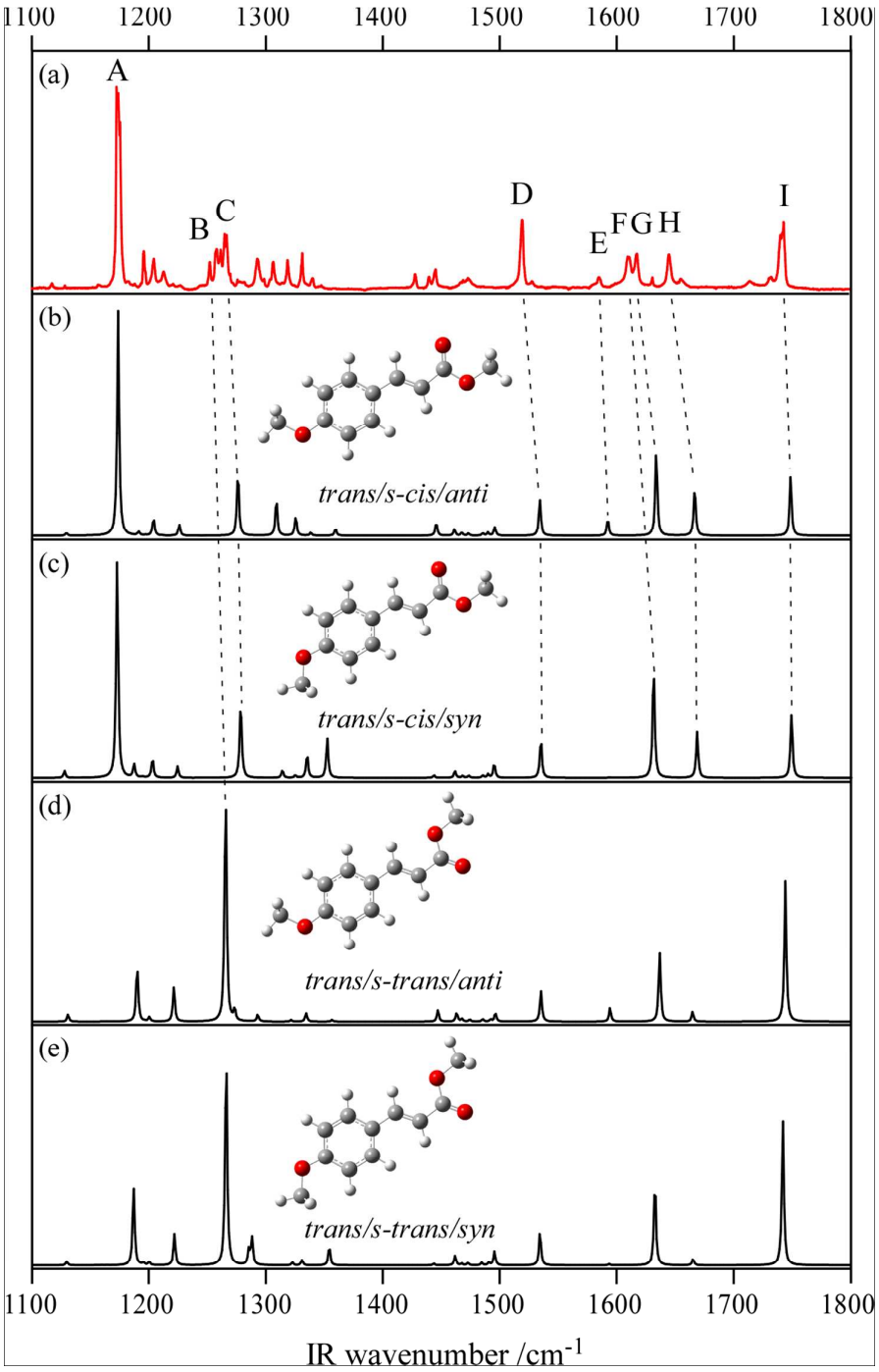

Figure 1. (a) IR spectrum of *p*-MMC deposited on the low-temperature Ne matrix without UV irradiation. The letters A - I indicate the major vibrational bands in the mid-IR region. (b)-(e) calculated IR spectra of *trans-p*-MMC conformers and molecular structures (inlet). A scaling factor of 0.9941 was applied to correlate the 1172 cm^{-1} band (band A) of the observed spectrum.

Table 1. Observed IR frequency in cm^{-1} and calculated IR frequencies in cm^{-1} of *trans-p*-MMC and the assigned vibrational mode (letter in red is the most contributed one)

	Expt.		Calc.				
	freq	Relative intensity	*s-cis/anti* (relative intensity)	*s-cis/syn* (relative intensity)	*s-trans/anti* (relative intensity)	*s-trans/syn* (relative intensity)	Vibrational mode
A	1172	100	1172 (100)	1172 (100)			C-O stretch (ester), O-Me wag (ester), C-H bend (prop), C-H bend (ring)
	1196	17	1190 (2)	1187 (6)	1190 (23)	1186 (40)	C-H bend (ring)
	1204	13	1203 (7)	1203 (7)	1200 (2)	1200 (2)	O-Me wag (ester), C-O stretch (ester)
	1212	7	1224 (5)	1224 (5)	1220 (16)	1220 (17)	C-H bend (prop), C(ring)-C(prop) stretch, C-H bend (ring)
B	1257	18			1264 (100)	1265 (100)	C-O stretch (ester), O-Me wag (ester), C-H bend (prop), C-H bend (ring), C-O stretch (ring)
C	1265	26	1274 (24)	1277 (28)			C-O stretch (ring), O-Me wag (ring), C-C stretch (ring), C-H bend (ring)
	1293	13	1308 (14)		1308 (16)		C(ring)-C(prop) stretch, C-C stretch (ring), C-H bend (ring), C-H bend (prop)
	1306	12	1324 (8)	1324 (8)	1320 (1)	1322 (1)	C-H bend (ring), C-H bend (prop)
	1318	12	1337 (1)	1335 (8)	1333 (4)	1330 (3)	C-H bend (prop), C-H bend (ring)
	1331	16		1352 (16)			C-H bend (prop), C-H stretch (ring), C-C stretch (ring)
	1340	4	1359 (3)		1355 (1)		C-H bend (prop), C-C stretch (ring), C-H bend (ring)
	1428	6	1445 (5)	1443 (1)	1445 (5)	1442 (1)	C-C stretch (ring), C-H bend (ring)
	1445	13	1460 (3)	1461 (3)	1470 (4)	1461 (5)	O-Me wag (ester)
	1472	3	1495 (4)	1495 (5)	1495 (4)	1495 (8)	O-Me wag (ring)
D	1519	32	1534 (16)	1535 (14)	1534 (14)	1533 (17)	C-H bend (ring), C-C stretch (ring), C-O stretch (ring), O-Me wag (ring)
E	1585	4	1592 (6)		1592 (6)		C-C stretch (ring), C-H bend (ring)
F	1610	14		1631 (41)		1632 (37)	C-C stretch (ring), C-H bend (ring), C(ring)-C(prop) stretch, C=C stretch (prop)
G	1617	16	1633 (36)		1635 (32)		C-C stretch (ring), C-H bend (ring), C(ring)-C(prop) stretch, C=C stretch (prop)
H	1645	15	1666 (19)	1668 (19)	1663 (5)	1665 (3)	C=C stretch (prop), C=O stretch (ester), C-C stretch (ring)
	1740	25			1743 (66)	1743 (75)	C=O stretch (ester), C=C stretch (prop), C-H bend (prop)
I	1742	32	1748 (26)	1748 (26)			C=O stretch (ester), C=C stretch (prop), C-H bend (prop)

Table 2. The calculated S_0 state stability of *trans*- and *cis*-*p*-MMCs in cm^{-1} including the zero-point energy correlation. The values in the parentheses are the relative energy among the *cis*-isomer.

	trans				*cis*			
	s-cis		*s-trans*		*s-cis*		*s-trans*	
	anti	*syn*	*anti*	*syn*	*anti*	*syn*	*anti*	*syn*
relative energy /cm^{-1}	0	57	295	363	1704 (53)	1651 (0)	2742 (1091)	2760 (1109)

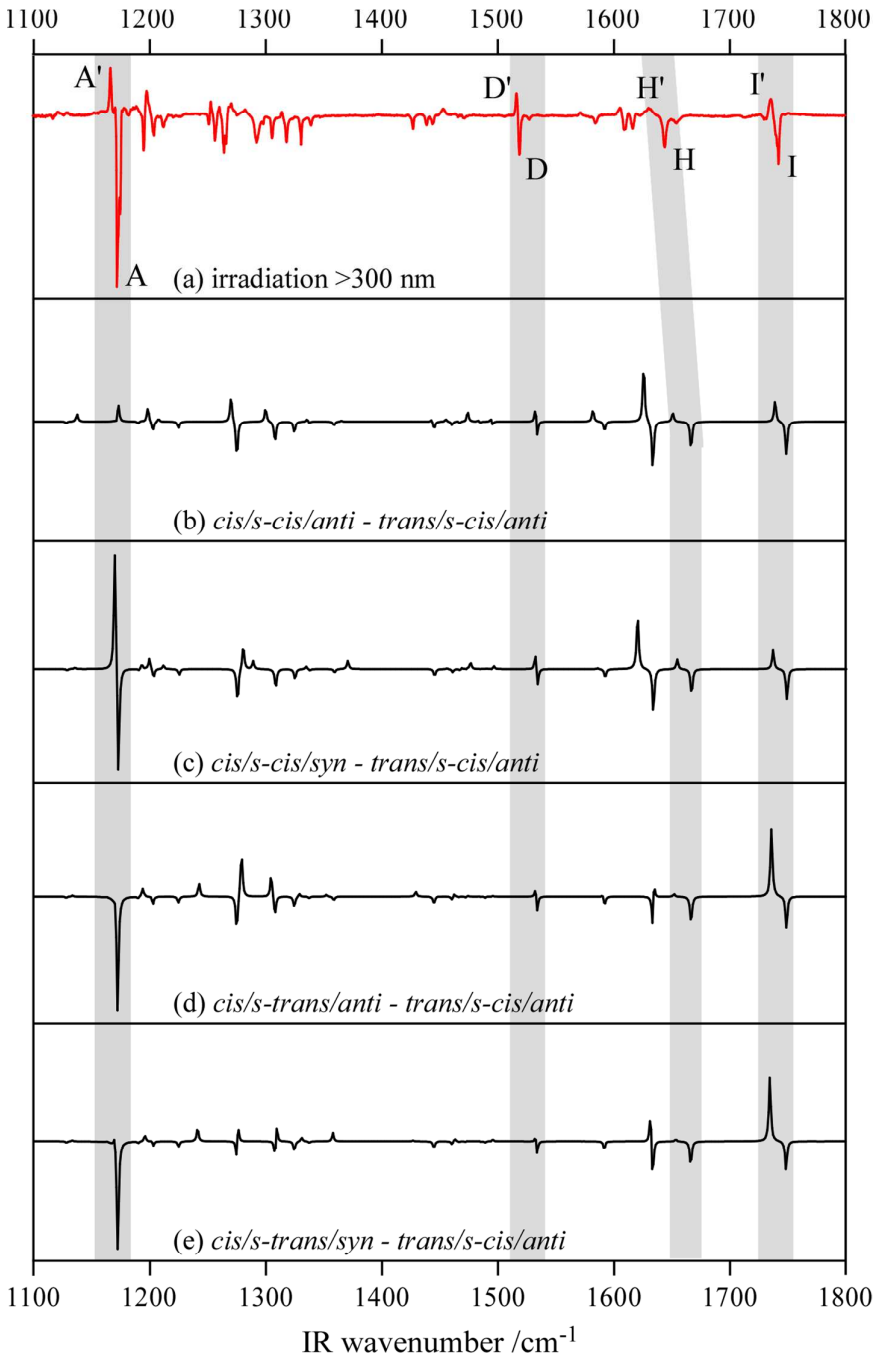

Figure 2. (a) Difference IR spectrum of *p*-MMC between the UV (> 300 nm) iradaited one and that before the UV irradiation, on the low-temperature Ne matrix. (b)-(e) calculated difference IR spectra of *p*-MMC obtained by subtracting the *trans/s-cis/anti* conformer from the *cis/s-cis/(anti or syn)* conformer. Each spectrum was scaled with a factor of 0.9941. The grey colored regions highlight the remarkable structural change.

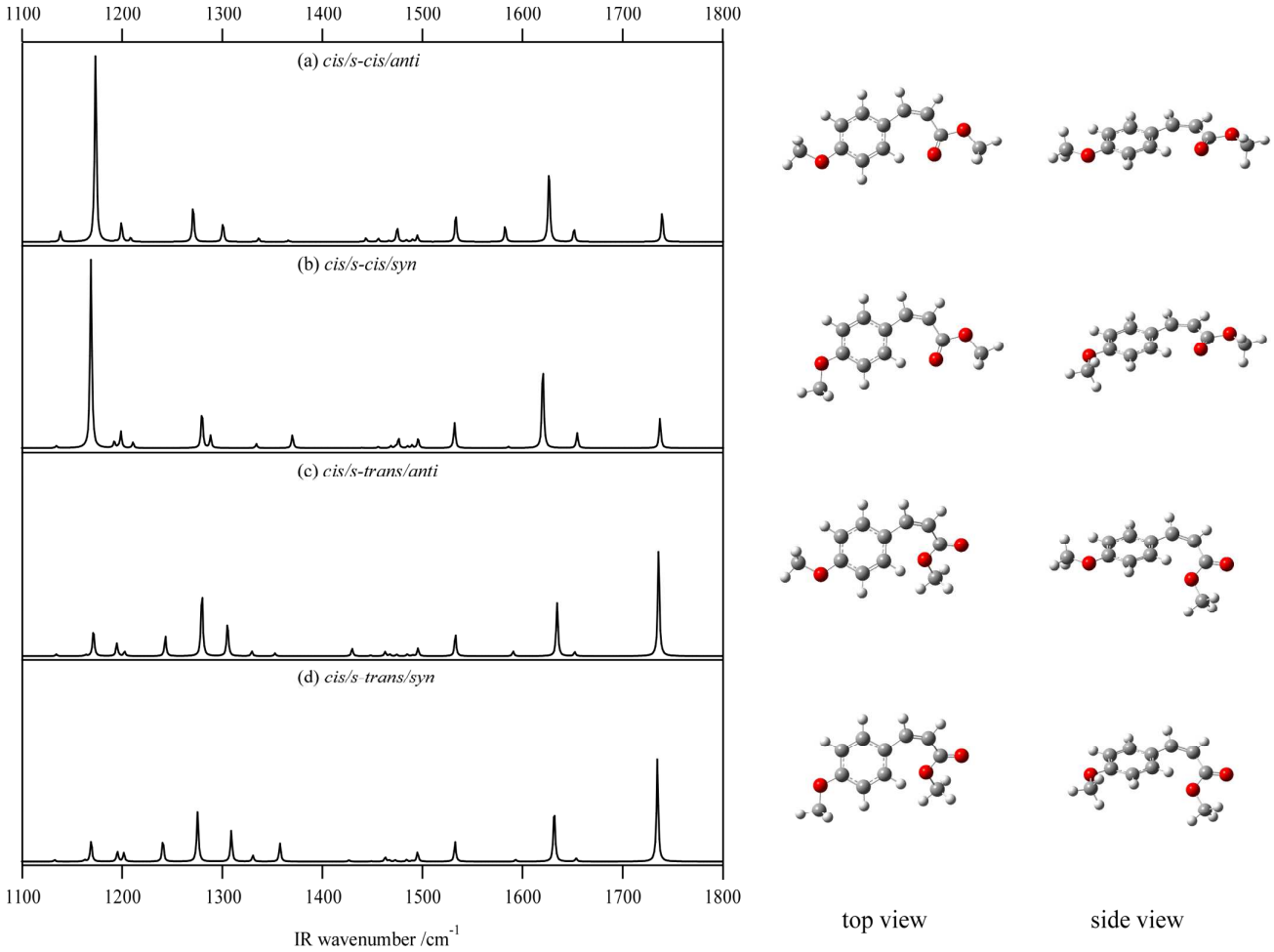

Figure 3. (a)-(d) Calculated IR spectra of *cis-p*-MMC conformers (left) and molecular structures with the top and side views (right).

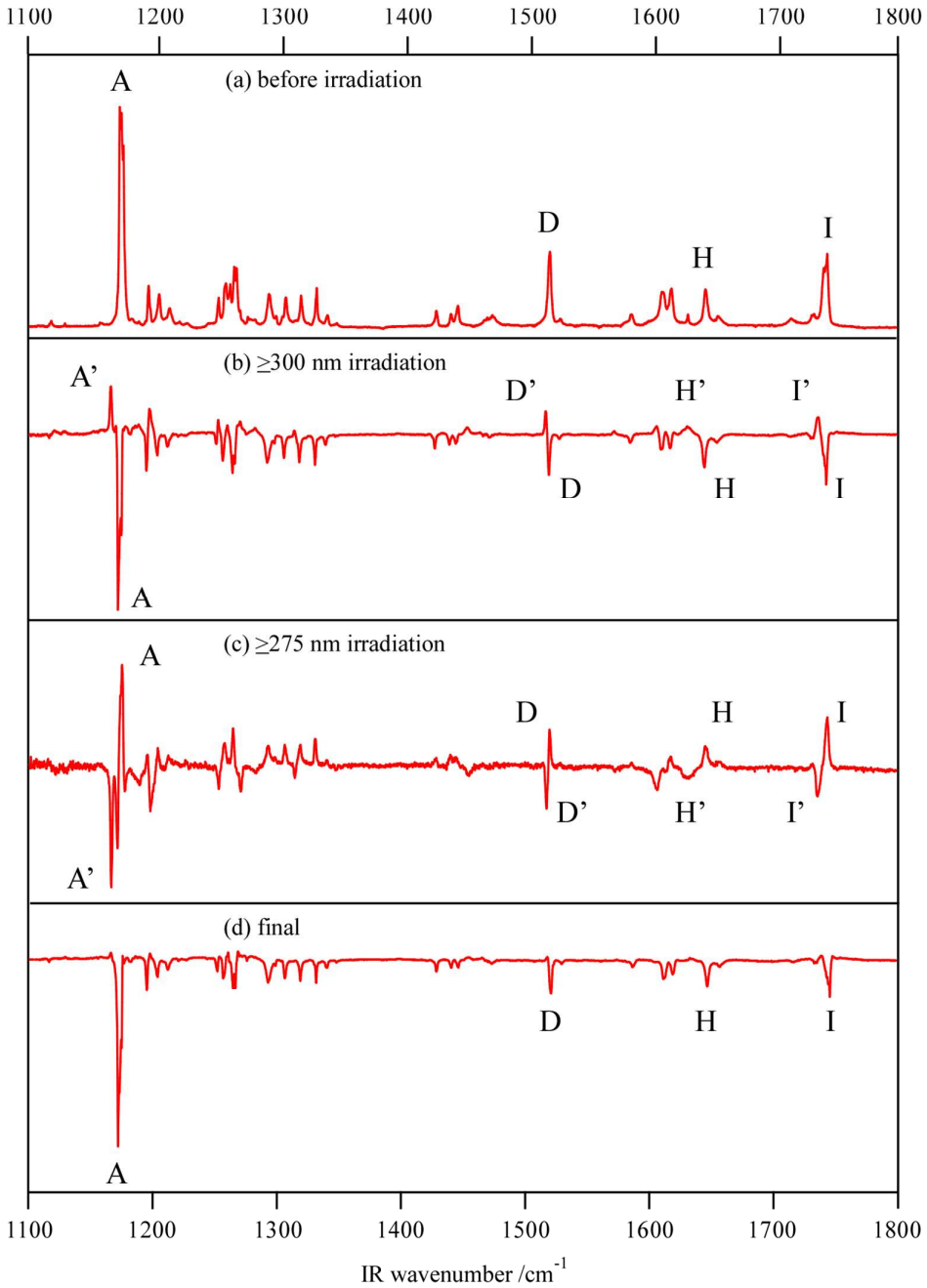

Figure 4. (a) IR spectrum of *p*-MMC before the UV irradiation. (b) Difference IR spectrum of *p*-MMC between the UV (> 300 nm) iradaited one and that before the UV irradiation. (c) ifference IR spectrum of *p*-MMC between the sequential UV (> 300 nm + > 275 nm) iradaited one and that of the UV (> 300 nm) irradaited. (d) Difference IR spectrum between (c) and (a).

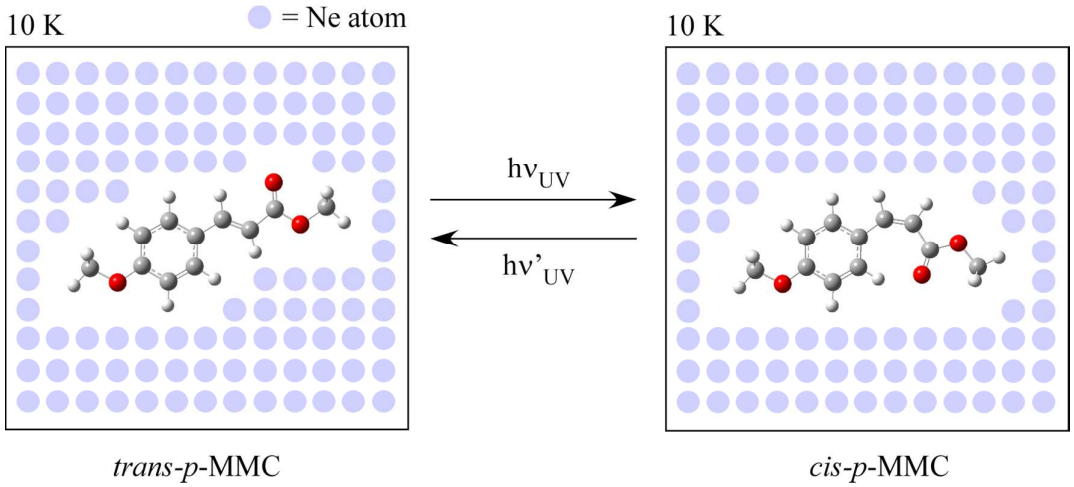

Table of Content